Motion-adaptive duty-cycling to estimate orientation using inertial sensors

Adrian Derungs[1,2], Han Lin[2], Holger Harms[3], Oliver Amft[1,2]
[1]Chair of Sensor Technology, University of Passau, Germany
[2]Signal Processing Systems, TU Eindhoven, The Netherlands
[3]Thales Defence and Homeland Security, Switzerland
{adrian.derungs,oliver.amft}@uni-passau.de

***Abstract*—We present a motion-adaptive duty-cycling approach to estimate orientation using inertial sensors. In particular, we deploy a proportional forward-controller to adjust the duty-cycle of inertial sensing units (IMU) and the orientation estimation update rate of an extended Kalman filter (EKF). In sample data recordings and a simulated daily life dataset from a wrist-worn IMU, we show that our motion-adaptive approach incurs substantially lower errors that a static duty-cycling approach. During phases with low or no rotation motion, as it is often occurring in daily activities, our approach can dynamically reduce the IMU operation to 20% of the regular rate. Results show that duty-cycles of 50% are common during low-wrist rotation activities, such as reading and typing, while orientation error is below 1°. We further show the power saving benefits of our approach in a case study of the ETHOS IMU device.**

I. Introduction

Inertial Measurement Units (IMUs) are widely used in wearable systems to determine orientation of the human body or limbs. IMUs typically consist of three sensor modalities, including acceleration, gyroscope, and magnetic field sensors, where each modality is implemented with three orientation axes. Orientation is often estimated from IMU data using extended Kalman filtering (EKF) [1]. IMU applications can be found in rehabilitation [2], [3], [4], gait analysis [5], gesture recognition [6], [7] and many others. Moreover, recent smartphones incorporate IMUs as motion-based interaction option for applications.

A major drawback of IMUs is the power consumption of sensors, in particular of gyroscopes, and power needed for computing orientation estimates from the nine inertial sensors. As a consequence, many commercial IMU devices, e.g. the Xsens MTw[1], have a limited runtime of 2-4 hours between battery recharges only. However, for wearable IMU systems, battery size should be small and runtime maximal to support continuous use in the applications mentioned before. While initial developments have been made to reduce to power consumption, e.g. for accelerometers [8], full IMU systems have received limited attention (see related work for more details). Shankar et al. [4] confirmed that duty-cycling could reduce power consumption in IMUs. However, plainly reducing sampling and orientation estimation rate would result in increased estimation errors. Orientation estimation errors are particularly critical during motion that involves rotations, e.g. for a drinking gesture, where the arm is turned to grab a cup. In contrast, many phases during everyday life involve limited or no limb or body turns, e.g. while typing on a keyboard. In such phases, the sampling and orientation estimation speed could indeed be reduced, i.e. as a low power operation mode. Many modern inertial sensor devices offer low-power and sleep states to support duty-cycling. Moreover, at reduced orientation estimate rate, the processing unit clock could be reduced too. Hence, a motion-adaptive control of the IMU duty-cycle and the subsequent orientation estimation rate could benefit system runtime.

In this paper, we present a motion-adaptive approach to duty-cycling the orientation estimation using an EKF. We deploy a proportional forward-controller to adjust the system's duty-cycle based on the current angular rate measured by the system's gyroscopes. Since the angular rate is related to the change in estimated orientation, our approach can be used to duty-cycle the IMU sampling frequency and the EKF orientation estimation speed. In this work, we focus on hand and arm motion, as used in many applications of IMU systems. In particular, we consider IMU systems worn at the wrist, e.g. as in a smart watch.

In particular, we make the following contributions:

1) We formally present our motion-adaptive approach to duty-cycle the IMU sampling and EKF orientation estimation rates. We detail how the forward controller is integrated into the EKF processing. Based on different toy data examples, we demonstrate the shortcomings of plain duty-cycle reductions on the orientation estimate accuracy and the performance of the motion-adaptive approach.
2) We evaluate our approach in (1) a toy dataset, consisting of isolated hand and arm motions, and (2) a simulated daily life dataset with several participants, considering office work, leisure activities, video gaming, and eating. We show that our motion-adaptive strategy is appropriate to adjust the duty-cycle and thus save power. In a case study, we illustrate the energy saving potential.

II. Related work

With the growing adoption of smartphone IMUs for activity recognition, power efficient sampling strategies where investigated. Yan et al. [8] presented an activity-sensitive strategy for continuous activity recognition. The accelerometer sampling frequency and the classification feature set was adapted

[1]http://www.xsens.com

dynamically after recognising activities. The results showed benefits for energy saving, but only considered accelerometers.

Priyantha et al. [9] investigated how to save energy while continuously processing phone sensor data. The authors designed an add-on device, termed *LittleRock* that could be plugged onto the phone and communicate with the mobile phone's processor through a serial interface. LittleRock consisted of a low-power processor to perform computations, while the mobile phone's processor is in sleep mode. In a demonstration, the authors showed a 70 times lower power consumption when using LittleRock for computation instead of the mobile phones processor. Their approach did not investigate orientation estimation, actual processing needs, and required to attach additional hardware to a mobile phone. Modern smartphones incorporate the concept of "big and little" processors in their design to save power by disabling the main processor during continuous routine operations, such as sensor sampling. Beside the main processor, e.g. Apple's iPhone 5s uses a M7 motion co-processor. The M7 is a ARM Cortex-M3 based controller that collects sensor data (accelerometers, gyroscopes, and magnetometer). Applications can access and process the stored data using the main processor. Our approach in this paper directly addresses the operation of low-power co-processors that are used in daily life activity recognition. By dynamically changing the duty-cycle, sample update rate of the sensors and the orientation estimation rates are adjusted to fit actual processing needs, e.g. of a subsequent motion analysis or recognition.

A. Power optimisation of inertial measurements

Our analyses of related works revealed that power optimisation of IMU systems received limited attention. The work of Shankar et al. [4] is closest to our approach. The authors investigated a gait assessment application, where duty-cycling was used to turn off the gyroscope for short time periods during power saving mode. In normal mode, the gyroscope ran at full system speed. Different sensor duty-ratios were set manually to evaluate energy saving potential. In a pilot simulation, a power saving of more than 60% was estimated. This result indicates the potential benefit of duty-cycling IMU devices. However, their investigation did not consider adaptive control of the duty-cycling. With our framework, we demonstrate that an adaptive controlled duty-cycle does not affect the orientation estimation and allows an optimal estimation performance.

Park et al. [10] computed angular rates with a gyroscope-free inertial measurement unit (GF-IMU) to reduce power consumption. An EKF was used to derive angular rate estimations to improve the GF-IMU performance. The authors compared their system to a conventional GF-IMU. While their results showed, that their GF-IMU performed superior to an conventional GF-IMU, no comparison to a full IMU was made.

A combination of power saving strategies for an IMU-based gait measurement system are described in [5]. A custom hardware with power optimised components-of-the-shelf was developed. Sleep modes were introduced to stop unused components when possible, e.g. the CPU after a computation, the RF module after a transmission, and unused gyroscope axes. Finally, gait parameters were computed on-board and sent directly to a host computer, instead of continuously sending raw data. Hence transmission time and power consumption were reduced.

Power consumption is not only an issue in IMUs. It is generally considered essential in Wireless Sensor Networks (WSN). WSNs typically expend energy in computation and data transmission. The lack of energy in some relevant sensor nodes can affect accurate data aggregation as well as the networks lifetime. WSNs typically operate by activating only needed nodes relevant to track/measure, while others are kept sleeping, e.g. [11], [12], [13]. While strategies to reduce power consumption in WSNs are relevant for wearable systems, we focus in this work on energy management within individual sensor nodes, as an IMU device.

B. Adaptive Kalman filtering

The Kalman filter uses a set of mathematical equations to estimate the state of a process from observations. The filter was used for various applications, including geodesy and vehicle navigation [14], [15], [16]. One derivative of the basic Kalman filter is the adaptive Kalman filter (AKF). AKFs have been developed using three different scenarios of adaptation: dynamic noise covariance matrix Q, measurement noise covariance matrix R, and the initial values of the error covariance matrix P [15]. In [17] an AKF was used to estimate position of post-stroke patients' movements. Several IMUs were attached to the patients upper limbs. A modified adaptive filtering algorithm was investigated, were additional variables were introduced to minimise the Mean Square Error.

In contrast, our work focuses on a control algorithm to reduce power consumption in IMUs. Our control considers forward information from angular rate measurements in order to dynamically adjust duty-cycles. We did not aim at modifying process and measurement noise in this work.

III. Motion-adaptive duty-cylcing concept

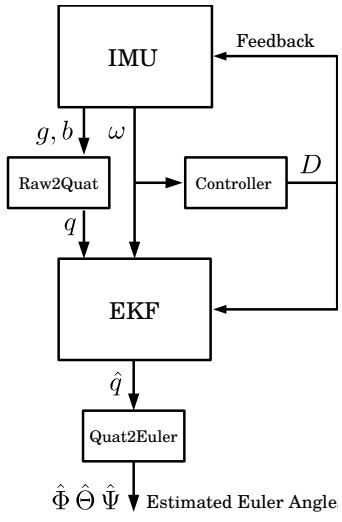

Fig. 1. Design of our motion-adaptive orientation estimation system. The angular rate (ω) is feed-forward into a duty-cycle rate controller. The controller provides a rate output (D) that controls IMU sampling rate and EKF processing rate. The data from the acceleration (g) and the magnetic field sensors (b) are used to derive quaternion coordinate pre-estimates (q). From the EKF quaternion coordinate estimates $\hat{q}$ are extracted and converted to Euler angles ($\hat{\Phi}$, $\hat{\Theta}$, and $\hat{\Psi}$).

We modified the standard configuration of a inertial sensing and orientation processing system by adding a controller to continuously monitor the estimation quality. When the system is effected by rotations, the orientation estimation rate should be increased up to the maximum system sampling rate. In contrast, if there are no rotations affecting the system, sampling and processing rates could both be reduced. During these sub-maximum duty-cycles, energy could be saved. The controller integration is a key aspect of the motion-adaptive system design. To minimise orientation estimation error, we chose a feed-forward control design, based on the angular rate measurements obtained from the IMU. Figure 1 illustrates the system design. Below, we provide an overview on the main system units.

Motion sensing IMU. As in a classic fixed-rate design, IMU provides samples from acceleration, gyroscope, and magnetic field sensors. The signals are commonly used to estimate orientation. The IMU device receives sample rate control from the duty-cycle controller (via the control signal D) to adjust the data rate provided to the further processing blocks.

Raw sensor data conversion (Raw2Quat). IMU sensor data is preprocessed and filtered to reduce measurement noise. Subsequently, raw orientation estimates are derived from acceleration and magnetic field sensors and converted to quaternion coordinates pre-estimates ($\boldsymbol{q}$).

Motion-adaptive rate control. A control unit receives the angular rate measurements ($\boldsymbol{\omega}$) from the three gyroscopes and produces a control signal $\boldsymbol{D}$ denoting the duty-cycling rate for subsequent processing of IMU and EKF.

Orientation estimation using EKF. The pre-estimated quaternion coordinates are combined with the angular rate measurements from the gyroscope sensors, resulting in a 7-state vector EKF design. The EKF processing rate is adjusted through the controller duty-cycle rate output.

Extracting orientation angles. As in a classic IMU-based orientation estimation design, estimates of quaternion coordinates ($\hat{\boldsymbol{q}}$ are extracted from the EKF state vector and converted to Euler angles $\hat{\boldsymbol{\Phi}}$, $\hat{\boldsymbol{\Theta}}$, and $\hat{\boldsymbol{\Psi}}$).

IV. Implementation

In this section, we detail the design of our motion-adaptive duty-cycling approach. In particular, we describe the processing rate control in the EKF, the proportional controller design, and the orientation representation formalism used.

A. EKF processing rate control

Our EKF needs to deal with dynamic sampling rate changes to accommodate variations in rotation rates. A detailed processing diagram of the EKF and its operations is presented in Figure 2, adapted from the fixed-rate EKF design proposed by Yun and Bachmann [1].

We used a linearised model with a discrete state transition matrix ($\boldsymbol{A}$), discrete measurement matrix ($\boldsymbol{H_k}$), discrete measurement noise covariance matrix ($\boldsymbol{R_k}$) and discrete process noise covariance matrix ($\boldsymbol{Q_k}$). We determined initial state estimates $\hat{\boldsymbol{x}}_{\boldsymbol{0}}^{-}$ and the discrete error covariance matrix ($\boldsymbol{P_0}$). In the EKF correction step the Kalman gain $\boldsymbol{K_k}$ is updated such that the posteriori error covariance is minimised. In the prediction step, the process model ($\boldsymbol{F}$) and the sampling time ($\boldsymbol{dt}$) is part to project the state ahead.

In the measurement update, new angular rate measurements ($\boldsymbol{\omega}$) are used to update the actual measurement $\boldsymbol{z_k}$. As measurement update vector, $\boldsymbol{z_k}$ contains the pre-estimated quaternion coordinates from acceleration and magnetic field sensors too. The residual error $\tilde{\boldsymbol{y}}$ is derived, reflecting the variation between the predicted measurement ($\boldsymbol{H}\hat{\boldsymbol{x}}_{\boldsymbol{k}}^{-}$) and the actual measurement $\boldsymbol{z_k}$. In our control approach, $\tilde{\boldsymbol{y}}$ could be considered as orientation estimation error measurement, hence to control the duty-cycle. However, we considered that computing $\tilde{\boldsymbol{y}}$ may delay the controller reaction at the onset of rapid motion. Hence, we chose to use the angular rate measurements ($\boldsymbol{\omega}$) as a most direct indicator of rotations. The disadvantage of using angular rates is their susceptibility to measurement noise that could influence the controller output. The EKF finally provides estimated quaternions $\hat{\boldsymbol{q}}$.

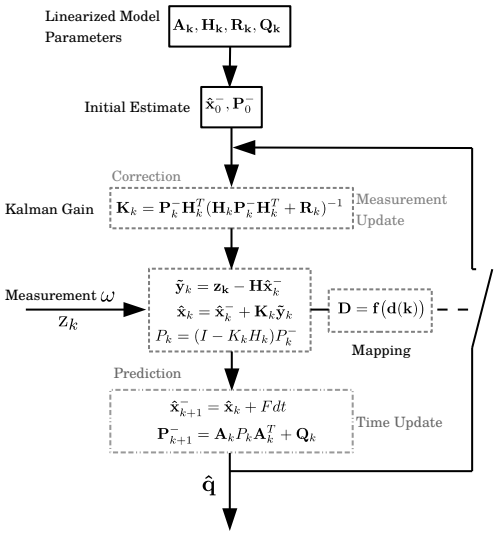

Fig. 2. Block diagram of the motion-adaptive EKF design. The orientation estimation rate is controlled via angular rate measurements obtained from the gyroscopes. The control operation is illustrated as a mapping function that produces the duty-cycle rate $\boldsymbol{D}$. This illustration was adapted from the fixed-rate EKF design proposed in [1].

B. Proportional controller design

To investigate the feasibility of our motion-adaptive approach, we chose a feed-forward proportional controller design. The controller aims at minimising both, the estimation error and the duty-cycle rate. We chose a feed-forward design and used the angular rate measurements $\boldsymbol{\omega}$ from the gyroscope sensors as control input. Thus, the controller can react upon rapid rotation changes by adjusting $\boldsymbol{D}$.

The proportional control input was derived as the maximum of the three-dimensional angular rate measurements $\boldsymbol{\omega}$:

$$\boldsymbol{d(k)} = \max\left(\boldsymbol{\omega_{X,k}^2}, \boldsymbol{\omega_{Y,k}^2}, \boldsymbol{\omega_{Z,k}^2}\right), \tag{1}$$

where $\boldsymbol{d}$ denotes the controller input and $\boldsymbol{k}$ is the time-step update.

We employed a linear mapping function to convert $\boldsymbol{d}$ to the duty-cycle rate $\boldsymbol{D}$. To deal with measurement noise in the angular rates, a flooring duty-rate ($\boldsymbol{D_{low}}$) at a threshold $\boldsymbol{d_{low}}$ was used. We further considered a ceiling duty rate ($\boldsymbol{D_{high}}$) at $\boldsymbol{d_{high}}$. $\boldsymbol{D_{low}}$ serves as lower processing speed limit of the system to ensure that rotations are detected. While $\boldsymbol{D_{low}}$ can be set as a system design parameter, $\boldsymbol{d_{low}}$ can be estimated from the gyroscope sensor noise observed. Furthermore, we fixed $\boldsymbol{D_{high}} = \mathbf{1}$ to permit the system to operate at its maximum frequency when needed.

To illustrate system performances, we used $\boldsymbol{d_{high}}$ to vary the proportional gain of the controller. When $\boldsymbol{d_{high}} = \boldsymbol{d_{low}}$, the controller would set $\boldsymbol{D} = \mathbf{1}$ for any estimation of $\boldsymbol{d}$ above the noise level. If $\boldsymbol{d_{high}} >> \boldsymbol{d}$, the controller will react with lower $\boldsymbol{D}$. In extreme settings for $\boldsymbol{d_{high}}$, duty-rate could be substantially reduced, while incurring potentially large orientation estimation errors. We chose the controller parameters by analysing the toy dataset (as introduced in Sec. V). The controller mapping function and proportional gain sweep is illustrated in Figure 3.

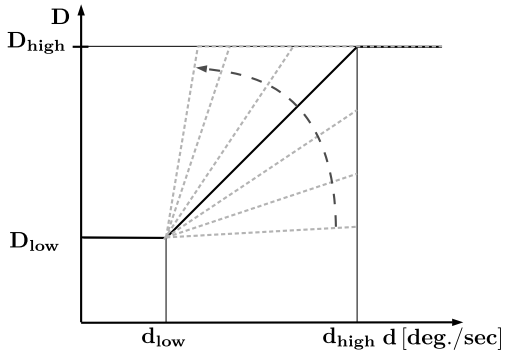

Fig. 3. Illustration of the proportional controller gain mapping. The controller input $\boldsymbol{d}$ was derived from the angular rate measurements (see main text). Dashed lines indicate the controller gain sweep used subsequently to analyse the performance of our motion-adaptive duty-cycling approach.

C. Orientation representation

Several orientation conversions are needed to estimate orientation angles in quaternion coordinates and Euler angles. In this work, we used Euler angles as the system's orientation output, while quaternion coordinates are used for processing in the EKF.

Orientation can be defined as a set of parameters that relates the angular position of a frame to another reference frame [18]. Euler angles are a common and intuitive way to describe orientation. The body orientation is denoted by the three angles $\boldsymbol{\Phi}$ (roll angle), $\boldsymbol{\Theta}$ (pitch angle) and $\boldsymbol{\Psi}$ (yaw angle) corresponding to angles around the three Cartesian axes *x*, *y* and *z*. The major drawback of this representation is its sensitivity to singularity. If $\boldsymbol{\Theta} = \pm\boldsymbol{\pi/2}$, the results becomes indefinite. Therefore, we did not use Euler angles for the EKF. Singularity issues can be avoided by applying quaternions. The quaternion representation uses four parameters ($\boldsymbol{q_1}, \boldsymbol{q_2}, \boldsymbol{q_3}, \boldsymbol{q_4}$) to describe orientation. Its mathematical definition and properties can be found in [18]. Due to their computational simplicity (no trigonometric computations needed) and the absence of possible undefined states, they are frequently preferred compared to Euler angles.

IMU sensors provide raw data from acceleration and magnetic field sensors in three gravity components ($\boldsymbol{g_x}, \boldsymbol{g_y}, \boldsymbol{g_z}$) and ($\boldsymbol{b_x}, \boldsymbol{b_y}, \boldsymbol{b_z}$) within the local frame. Acceleration components were used to compute the roll angle $\boldsymbol{\Phi}$ and pitch angle $\boldsymbol{\Theta}$. From magnetic field data the yaw angle $\boldsymbol{\Psi}$ was derived. When the IMU is not tilted, Euler angles can be calculated by:

$$\begin{aligned} \boldsymbol{\Phi} &= \boldsymbol{arctan}(g_y/g_z) \\ \boldsymbol{\Theta} &= -\boldsymbol{arctan}(g_x/g) \\ \boldsymbol{\Psi} &= \boldsymbol{arctan2}(b_y, b_x) \end{aligned} \tag{2}$$

For a tilted IMU, tilt compensation techniques were used to convert inclined measurements into a horizontal plane. This approach is suitable for static motions with low dynamics. During high dynamics, i.e. limb rotations, all orientation agles are distorted as consequence of occuring accelerations. The EKF was used in this work to combat the distortions, by combining orientation pre-estimates from acceleration and magnetic field sensors with angular rate measurements from gyroscopes.

A complete description of the EKF is beyond the scope of this paper. The work of Bishop and Welch [19] provides an overview on the EKF approach. In our work, a seven state extended Kalman filter was used to handle a non-linear dynamical system. We followed the design for a fixed-rate EKF of Yun and Bachman [1] with the modifications stated above. The state vector, denoted by $\vec{\boldsymbol{x}}$ includes four quaternions coordinates $\boldsymbol{q}$ and three angular rate components ($\boldsymbol{\omega}$):

$$\boldsymbol{\omega} = \begin{bmatrix} \boldsymbol{x_1} \\ \boldsymbol{x_2} \\ \boldsymbol{x_3} \end{bmatrix} = \begin{bmatrix} \boldsymbol{p} \\ \boldsymbol{q} \\ \boldsymbol{r} \end{bmatrix}, \qquad \mathbf{q} = \begin{bmatrix} \boldsymbol{x_4} \\ \boldsymbol{x_5} \\ \boldsymbol{x_6} \\ \boldsymbol{x_7} \end{bmatrix} = \begin{bmatrix} \boldsymbol{q_1} \\ \boldsymbol{q_2} \\ \boldsymbol{q_3} \\ \boldsymbol{q_4} \end{bmatrix}. \tag{3}$$

The state equations, with $\boldsymbol{\tau}$ as time constant, are:

$$\begin{bmatrix} \dot{\boldsymbol{x_1}} \\ \dot{\boldsymbol{x_2}} \\ \dot{\boldsymbol{x_3}} \end{bmatrix} = \frac{\mathbf{1}}{\boldsymbol{\tau}} \left(- \begin{bmatrix} \boldsymbol{x_1} \\ \boldsymbol{x_2} \\ \boldsymbol{x_3} \end{bmatrix} + \begin{bmatrix} \boldsymbol{w_1} \\ \boldsymbol{w_2} \\ \boldsymbol{w_3} \end{bmatrix} \right) \tag{4}$$

$$\begin{bmatrix} \dot{\boldsymbol{x_4}} \\ \dot{\boldsymbol{x_5}} \\ \dot{\boldsymbol{x_6}} \\ \dot{\boldsymbol{x_7}} \end{bmatrix} = \frac{\mathbf{1}}{\mathbf{2}} \begin{bmatrix} \boldsymbol{x_4} \\ \boldsymbol{x_5} \\ \boldsymbol{x_6} \\ \boldsymbol{x_7} \end{bmatrix} \otimes \begin{bmatrix} \mathbf{0} \\ \boldsymbol{x_1} \\ \boldsymbol{x_2} \\ \boldsymbol{x_3} \end{bmatrix}. \tag{5}$$

V. Evaluation

To evaluate the motion-adaptive duty-cycling approach, we considered two different datasets, where a wrist-worn IMU was used by participants.

A. Toy dataset

We recorded a toy dataset with one participant wearing the IMU and performing different motions, as summarised in Table I. Each motion lasted for 30 to 160 s and was sampled with a frequency of 50 Hz. We used an MTw sensor unit (Xsens Technologies B.V.) and worn at the right wrist all recordings, except the *bow* motion.

TABLE I. TOY DATASET MOTIONS AND DESCRIPTION.

Motion	Description
Bow	90 ° bow with sensor affixed on the back of body.
Applaud	Applaud with approximately 0.7 s periodicity.
Draw cycle	Draw a circle clockwise in the air with arm motion
Bicep curl	Dumbbell bicep curl with a motion periodicity of approx. 2 s.
Read	Read a book with occasional page flipping.
Type	Type and occasionally stretch and take a sip of tea.
Drink	Grasp a cup, drink, and return the cup.

B. Daily life activity dataset

We further evaluated our approach using a dataset that consists of daily life activities recorded with a wrist-worn motion sensor. The dataset was recorded and presented in an earlier work [7]. Here we summarise the study methodology briefly. Seven students were included in the scripted recordings, including several daily routines, such as office work, leisure activities, video gaming, and eating. Among other sensors, participants wore a MTx sensor (Xsens Technologies B.V.) at the right wrist, sampled at 50 Hz. One recording session per participant of $\sim$ 60 min was used in our analysis.

The participants were instructed to perform different activities according to a defined task list, but were free to reorder activities and perform activities according to their accustomed habits. Further study details can be found in [7].

C. Performance evaluation

We evaluated the motion-adaptive duty-cycling algorithm performance by computing the root-mean-square error (RMSE) for each estimated Euler angle ($\mathbf{\Phi}$, $\mathbf{\Theta}$ and $\mathbf{\Psi}$) against the non-adaptive ($\boldsymbol{D = 1}$) orientation estimate $\boldsymbol{a_{ref}}$. We used the RMSE for any Euler angle $\boldsymbol{a_{est}}$ as follows:

$$\boldsymbol{RMSE = \sqrt{\frac{\sum_i^N \left(a(i)_{ref} - a(i)_{est}\right)^2}{N}}} \qquad (6)$$

where index $\boldsymbol{i}$ denotes estimation samples and $\boldsymbol{N}$ the observation length. For reduced duty-cycle rates ($\boldsymbol{D < 1}$), the latest estimation was considered at sample $\boldsymbol{i}$. RMSE was computed separately for each Euler angle ($\mathbf{\Phi}$, $\mathbf{\Theta}$, and $\mathbf{\Psi}$).

VI. RESULTS

We initially investigated the effect of fixed duty-cycling on the orientation estimation performance and the motion-adaptive control. Subsequently, we analyse the fixed duty-cycling and motion-adaptive control performance for the toy dataset. Finally, we show the motion-adaptive control performance for the daily life dataset.

A. Effect of duty-cycling and motion-adaptive control

Figure 4 shows the Euler angles of a typical drink gesture from our toy dataset, at full rate ($\boldsymbol{D = 1}$) and at fixed duty-cycles with $\boldsymbol{D < 1}$. As these example plots indicate, the angle variation decreases with lower $\boldsymbol{D}$, thus the orientation estimation error increases. This illustration confirms that a plain duty-cycle reduction would increase estimation errors, in particular for phases with rotation variation.

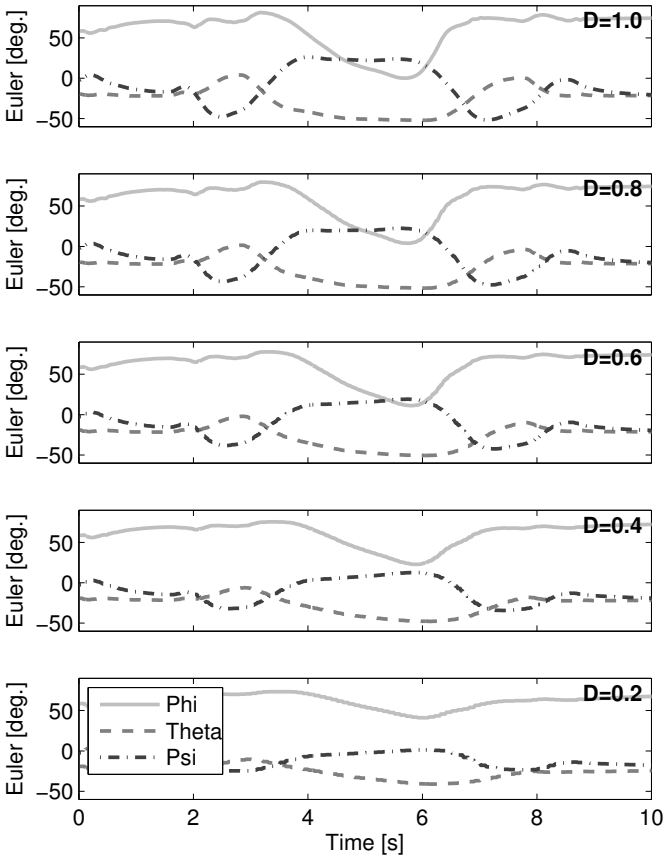

Fig. 4. Effect of fixed rate duty-cycling for an example drink gesture. The illustration shows different duty-cycle ratios ($\boldsymbol{D}$), where $\boldsymbol{D = 1}$ indicates the full-rate orientation estimation.

The performance of our motion-adaptive duty-cycle algorithm is shown in Figure 5. In the top panel, a visual overlay of the Euler angles for the adaptive estimation and the full-rate configuration is shown. All Euler angles exhibit a dynamically changing RMSE below 2.5° on average. The RMSE is shown in Table II. The $\mathbf{\Phi}$ angle showed the largest peak RMSE of $\sim$ 6°. Finally, the bottom panel shows the dynamically adaptive duty cycle rate $\boldsymbol{D}$. As the plot shows, the duty cycle drops to $\boldsymbol{D = 0.2}$, which corresponds to the $\boldsymbol{D_{low}}$ setting. In data segments with large rotation variance, $\boldsymbol{D}$ was increased as expected. On average, we measured $\boldsymbol{\bar{D} = 0.71}$.

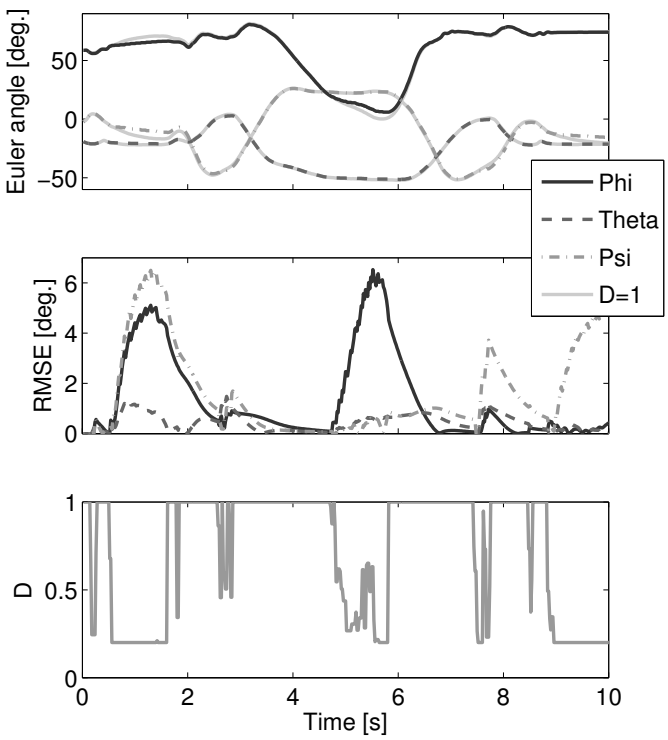

Fig. 5. Illustration of the motion-adaptive duty-cycling for an example drink gesture. Top panel: Overlay of the motion-adaptive orientation estimation and the full-rate ($\boldsymbol{D} = \mathbf{1}$) Euler angles. Mid panel: Dynamic RMS error for each Euler angle. Bottom panel: Dynamically adaptive duty-cycle ratio ($\boldsymbol{D}$).

TABLE II. SUMMARY OF THE AVERAGE RMSE FOR THE EXAMPLE DRINK GESTURE SHOWN IN FIG. 5.

Error	Value [deg./sec]
RMS $\boldsymbol{\Phi}$	2.2
RMS $\boldsymbol{\Theta}$	0.55
RMS $\boldsymbol{\Psi}$	2.39

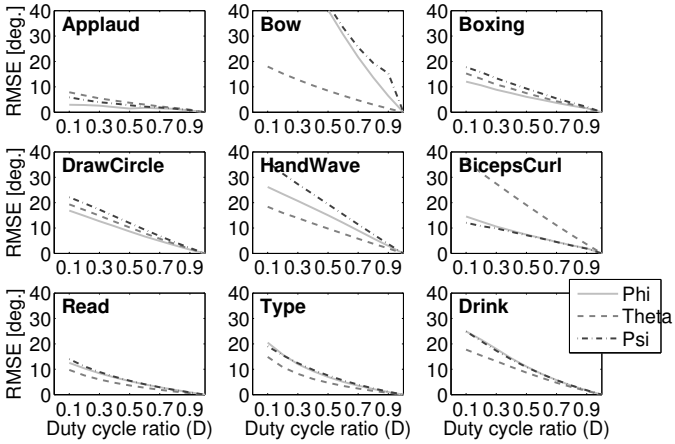

Fig. 6. Influence of different duty-cycle ratios (D) on the RMSE for each motion of the toy dataset.

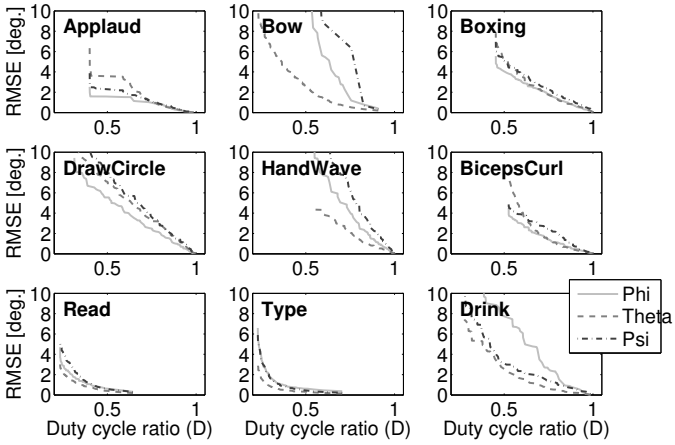

Fig. 7. RMSE-duty rate plot created by a controller gain sweep for the toy dataset motions. Our motion-adaptive approach provides benefits for motion that includes phases without rotations, such as reading and typing in this example.

B. Performance for toy dataset

For the toy dataset, we initially investigated the relation of RMSE and duty-cycle rate $\boldsymbol{D}$. Figure 6 shows the RMSE for all motions. The analysis shows that reducing duty-cycle even to $\boldsymbol{D} = \mathbf{0.8}$ incurs an RMSE above 5 to 10° in most motions. It can be observed that for motions with high dynamics (e.g. bow) the RMS error is larger than for other motions (e.g. read and type).

In Figure 7 we varied the controller gain by sweeping $\boldsymbol{d_{high}}$, as described earlier. This result demonstrates that our motion-adaptive approach can adjust the duty-cycle according to the individual update rate of each gesture. Here in particular, reading and typing motions benefit. The duty ratio can be set to $\boldsymbol{D} = \mathbf{0.5}$, while retaining a RMSE below 1-2°. Setting $\boldsymbol{D} = \mathbf{0.5}$ results in 50% of the original sampling rate, hence 25 Hz while achieving an accurate orientation estimation. At 25 Hz, the time between samples is 40 ms which is sufficient for many IMU devices to put sensors to sleep mode.

C. Performance for daily life activity dataset

Figure 8 shows the motion-adaptive performance in a RMSE-duty rate plot, created by a controller gain sweep. The diagram was created by averaging RMSE and duty rates across all participant recordings. Even for this complex dataset, an RMSE below 2° was achieved for an average duty-cycle rate of $\boldsymbol{D} < \mathbf{0.8}$. Since the recording contained many gesture instances and phases with wrist rotations, this result confirms that the motion-adaptive approach can be used for real-life data too.

VII. CASE STUDY - ETHOS IMU

To evaluate the energy saving potential of our motion-adaptive duty-cycling approach we further considered a hardware case study. In particular, we analyse the ETHOS IMU that contains a 16-bit dsPIC (MICROCHIP, dsPIC33FJ128) [20]. We provide a first estimation about power saving of the

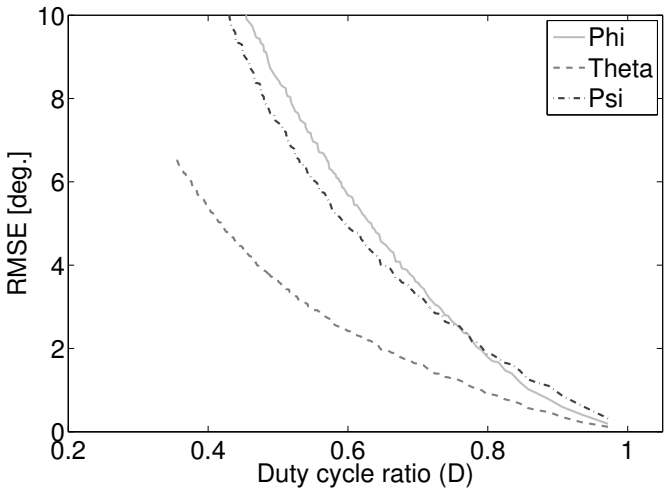

Fig. 8. RMSE-duty rate plot created by a controller gain sweep for the daily life activity dataset. In this analysis, the RMSE and duty rate result were averaged for all participants.

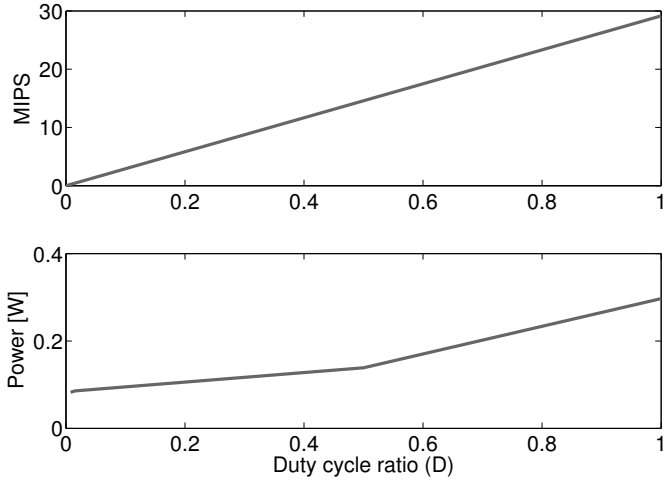

Fig. 9. MIPS and power requirements vs. duty-cycle rate ($\boldsymbol{D}$). We based our estimation on parameters derived from the ETHOS IMU design [20].

CPUs, due to the reduced processing effort needed for the adaptive EKF. Figure 9 shows in the top panel MIPS (million instructions per second) with respect to $\boldsymbol{D}$. The MIPS increase linear with an increased $\boldsymbol{D}$. Regarding our results, indicating a minimal $\boldsymbol{D}$ of 0.5 is feasible, 14.5 MIPS are needed for one orientation estimation calculation.

If the EKF operates at full duty-cycle ($\boldsymbol{D = 1}$), we assume a sampling frequency (Fs) of 50 Hz for a sufficient orientation estimation for motions with low or no rotation (reading and typing). According to Shannons theorem, this means a reproducible motion estimation is only possible for motion with a maximum cut-off frequency of 25 Hz. For $\boldsymbol{D < 1}$ the sampling frequency decrease with $\boldsymbol{D}$, e.g., if $\boldsymbol{D = 1}$ then Fs is 50 Hz, if $\boldsymbol{D = 0.5}$ then Fs is 25 Hz and so on. From the original ETHOS design [20] we derived the instruction cycles required per orientation estimation (486 k cycles). Hence for every $\boldsymbol{D}$ the MIPS can be calculated including an additional overhead of 20% representing internal CPU loads. An increased $\boldsymbol{D}$ means an increased number of samples and finally a higher amount of MIPS required:

$$\boldsymbol{MIPS = Fs \cdot 486\,\text{kcycles}/Estimation \cdot 1.2} \quad (7)$$

The second plot shows the power consumption as function of $\boldsymbol{D}$. To calculate the CPUs power consumption, we use data provided by the data-sheet. Since a duty-ratio of 0.5 is sufficient for an orientation estimation during reading and typing, we can predict a power reduction from 0.4 W to 0.14 W which is 35%. Even for the daily life dataset, we could save processing power already. Additional power reduction benefits could be expected from the IMU sensor sleep mode operation.

VIII. Discussion

Our first analysis of scaling fixed duty-cycling ratios demonstrated the limitations of duty cycling. With reduced $\boldsymbol{D}$, the EKF models the expected value of orientation angles. Considering the EKF estimation approach, the expected value (signal average) is the best estimator when samples are sparse and less informative. This result underlines the relevance of our approach to dynamically adapt the duty cycle rate.

Our subsequent investigation showed that the motion-adaptive approach using angular rates as feed-forward input to a proportional controller can reproduce the full-rate estimation at low RMSE. Using the toy dataset, we were able to illustrate opportunities to indeed save computational cycles and sampling effort. In particular, for activities involving low or no rotational motion, such as reading and typing, our motion-adaptive approach could reduce the average duty rate to $\boldsymbol{D = 0.5}$ or less, at an RMSE of below 1°. This result represents a key benefit of our method.

We observed that for more complex motion, such as the drinking gesture considered in the toy dataset, the controller could not pick up gradual changes in rotations adequately, resulting in sporadic RMSE up to 5°. It can be expected that further optimisation of the control approach could help to reduce the error. In particular, we plan to evaluate our approach in a larger daily life activity dataset with natural motion performance.

IX. Conclusion and further work

In this work we introduced a modified motion-adaptive duty-cycling approach for orientation estimation using inertial sensors. Our approach dynamically adjusts the duty-cycle of inertial measurement units (IMU) and the update rate of an extended Kalman filter (EKF). While using our motion-adaptive approach with a forward-controller rather a static duty-cycling approach, we show substantially lower errors for orientaion estimations.
In further work we attempt to model the electrical characteristics into our system. This allows a more precise characterization of the systems architecture to describe the power consumption. The duty-ratio influences the Root Mean Square

Error (RMSE) of the orientation estimation as well as the power consumption. The relation between the RSME and the enegy consumption is of prticular interest. Thus we can immediately assume whether we can save energy with minimum loss in accuracy, or not.
Further the motion itself needs careful considerations. The maximal cut-off frequency of an induvidual motion determines the minimal sampling frequency according to the sampling theorem of Shannon and Nyquist. If this cut-off frequencies are known, we can adjust our forward controller in a defined range.

X. Acknowledgements

This work was supported by the EU FP7 Marie Curie Network iCareNet under grant number 264738.

References

[1] X. Yun and E. R. Bachmann, "Design, implementation, and experimental results of a quaternion-based kalman filter for human body motion tracking," *Robotics, IEEE Transactions on*, vol. 22, no. 6, pp. 1216–1227, 2006. [Online]. Available: http://ieeexplore.ieee.org/xpls/abs_all.jsp?arnumber=4020379

[2] H. Zhou and H. Hu, "Human motion tracking for rehabilitation - a survey," *Biomedical Signal Processing and Control*, vol. 3, no. 1, pp. 1–18, 2008. [Online]. Available: http://www.sciencedirect.com/science/article/pii/S1746809407000778

[3] K. Nagarajan, N. Gans, and R. Jafari, "Modeling human gait using a kalman filter to measure walking distance," in *Proceedings of the 2nd Conference on Wireless Health*. ACM, 2011, p. 34. [Online]. Available: http://dl.acm.org/citation.cfm?id=2077584

[4] P. S. U. Shankar, N. Raveendranathan, N. R. Gans, and R. Jafari, "Towards power optimized kalman filter for gait assessment using wearable sensors." in *Wireless Health*, I. M. Jacobs, P. Soon-Shiong, E. Topol, and C. Toumazou, Eds. ACM, 2010, pp. 137–144. [Online]. Available: http://dblp.uni-trier.de/db/conf/wh/wh2010.html#ShankarRGJ10

[5] S. Zhu, H. Anderson, and Y. Wang, "Reducing the power consumption of an imu-based gait measurement system," in *Advances in Multimedia Information Processing–PCM 2012*. Springer, 2012, pp. 105–116. [Online]. Available: http://link.springer.com/chapter/10.1007/978-3-642-34778-8_10

[6] J. C. Lementec and P. Bajcsy, "Recognition of arm gestures using multiple orientation sensors: Gesture classsification," in *Proceedings of the 7th International IEEE Conference on Intelligent Transportation Systems*, October 2004, pp. 965–970.

[7] O. Amft, D. Bannach, G. Pirkl, M. Kreil, and P. Lukowicz, "Towards wearable sensing based assessment of fluid intake," in *PerHealth 2010: Proceedings of the First IEEE PerCom Workshop on Pervasive Healthcare*. IEEE, 2010, pp. 298–303.

[8] Z. Yan, V. Subbaraju, D. Chakraborty, A. Misra, and K. Aberer, "Energy-efficient continuous activity recognition on mobile phones: An activity-adaptive approach," in *ISWC 2012: Proceedings of the 2012 16th Annual International Symposium on Wearable Computers*, ser. ISWC '12. Washington, DC, USA: IEEE, 2012, pp. 17–24.

[9] B. Priyantha, D. Lymberopoulos, and J. Liu, "Enabling energy efficient continuous sensing on mobile phones with littlerock," in *IPSN 2010: Proceedings of the 9th ACM/IEEE International Conference on Information Processing in Sensor Networks*, ser. IPSN 2010. New York, NY, USA: ACM, 2010, pp. 420–421.

[10] S. Park, C.-W. Tan, and J. Park, "A scheme for improving the performance of a gyroscope-free inertial measurement unit," *Sensors and Actuators A: Physical*, vol. 121, no. 2, pp. 410–420, 2005. [Online]. Available: http://www.sciencedirect.com/science/article/pii/S0924424705001366

[11] X. Wang, J.-J. Ma, S. Wang, and D.-W. Bi, "Prediction-based dynamic energy management in wireless sensor networks," *Sensors*, vol. 7, no. 3, pp. 251–266, 2007. [Online]. Available: http://www.mdpi.com/1424-8220/7/3/251

[12] *Energy Efficient Prediction-Based Clustering Algorithm for Target Tracking in Wireless Sensor Networks*, 2010. [Online]. Available: http://ieeexplore.ieee.org/stamp/stamp.jsp?tp=&arnumber=5702112

[13] *Towards Energy-Efficient Algorithm-Based Estimation in Wireless Sensor Networks*, 2010. [Online]. Available: http://ieeexplore.ieee.org/stamp/stamp.jsp?tp=&arnumber=5714474

[14] C. Hu, W. Chen, Y. Chen, and D. Liu, "Adaptive kalman filtering for vehicle navigation," *Journal of Global Positioning Systems*, vol. 2, no. 1, pp. 42–47, 2003.

[15] A. Almagbile, J. Wang, and W. Ding, "Evaluating the performances of adaptive kalman filter methods in gps/ins integration," *Journal of Global Positioning Systems*, vol. 9, no. 1, pp. 33–40, 2010.

[16] A. Mohamed and K. Schwarz, "Adaptive kalman filtering for ins/gps," *Journal of Geodesy*, vol. 73, no. 4, pp. 193–203, 1999. [Online]. Available: http://link.springer.com/article/10.1007/s001900050236

[17] Y. Zhang, H. Hu, and H. Zhou, "Study on adaptive kalman filtering algorithms in human movement tracking," in *Information Acquisition, 2005 IEEE International Conference on*. IEEE, 2005, pp. 5–pp. [Online]. Available: http://ieeexplore.ieee.org/xpls/abs_all.jsp?arnumber=1635045

[18] J. L. Marins, X. Yun, E. R. Bachmann, R. B. McGhee, and M. J. Zyda, "An extended kalman filter for quaternion-based orientation estimation using marg sensors," in *Intelligent Robots and Systems, 2001. Proceedings. 2001 IEEE/RSJ International Conference on*, vol. 4. IEEE, 2001, pp. 2003–2011. [Online]. Available: http://ieeexplore.ieee.org/xpls/abs_all.jsp?arnumber=976367

[19] G. Bishop and G. Welch, "An introduction to the kalman filter," *Proc of SIGGRAPH, Course*, vol. 8, pp. 27 599–3175, 2001.

[20] H. Harms, O. Amft, R. Winkler, J. Schumm, M. Kusserow, and G. Troester, "Ethos: Miniature orientation sensor for wearable human motion analysis," in *Sensors 2010: Proceedings of IEEE Sensors conference*. IEEE, 2010, pp. 1037–1042.